UNCECOMP 2015
1st ECCOMAS Thematic Conference on
International Conference on Uncertainty Quantification in
Computational Sciences and Engineering
M. Papadrakakis, V. Papadopoulos, G. Stefanou (eds.)
Crete Island, Greece, 25–27 May 2015

UNCERTAINTY IN THE MOTION-EXCITED FORCES ON A SQUARE PRISM AND PROBABILISTIC ASSESSMENT OF GALLOPING INSTABILITY

L. Banfi[1], **L. Carassale**[2]

[1] University of Genova
via Montallegro 1, 16145, Genova, Italy
e-mail: lorenzo.banfi@dicca.unige.it

[2] University of Genova
via Montallegro 1, 16145, Genova, Italy
e-mail: luigi.carassale@ unige.it

Keywords: Galloping, Quasi-steady theory, Unsteady theory.

Abstract. *Galloping is an aeroelastic phenomenon typical of slender structures that can produce large-amplitude oscillations in cross-flow direction. Several structures typical of civil and mechanical engineering applications, e.g. cables and bracings exposed to a flow, may be prone to galloping and their reliability depends on the correct estimation of the critical conditions for which this instability can occur. Usually, the instability condition is characterized in terms of critical flow velocity, which depends on the aerodynamic behavior of the structure, as well as on its mechanical properties.*

The critical velocity can be estimated, indirectly, from aerodynamic tests involving force or pressure measurements on static bodies or on rigid structures oscillating according to a prescribed motion. This gives rise to large uncertainties due to the experimental conditions that are not perfectly controllable, the observation time that is necessarily limited and the models used to fit the data that do not reproduce perfectly the physics of the problem. These uncertainties reflects into inaccuracies in the evaluation of the critical instability condition.

In order to investigate the technical problem described above, an experimental campaign involving pressure measurements on a square cylinder with controlled harmonic motion in a bi-dimensional flow has been carried out. Motion excited forces have been modeled as random variables and characterized by statistical analysis of the experimental data. Finally, the probability of occurrence of the instability condition has been evaluated by propagating the experimental uncertainties through the traditional quasi-steady galloping approach, as well as through an unsteady formulation.

1 INTRODUCTION

Galloping is a well-known aeroelastic instability involving large amplitudes in the cross-flow direction. Several civil engineering structures with particular compact cross-section with non-circular shape, as iced power line cables and slender bodies like bracing, are particular sensitive to this phenomenon. A correct determination of the instability conditions is then a crucial aspects in the design process in order to avoid instable motions which can easily lead to the collapse of the structure.

The instability conditions are generally defined by a critical flow velocity, which depends on the aerodynamic properties of the cross section of the body, as well as on its mechanical properties. Many cross section shapes have been deeply investigated in the last years. In particular, the square cross section has received great attention in the aerodynamic field since the pioneering work by Parkinson and Smith [1], due to its particular susceptibility to galloping and its large use in many mechanical and civil engineering applications.

Even for the square cross section, the critical galloping conditions cannot be easily determined in an analytical way, requiring an experimental investigation. Through wind tunnel tests on static bodies in a smooth or turbulent flow the static aerodynamic properties as lift and drag coefficients, for different angles of attack, can be evaluated. A galloping coefficients function of lift and drag coefficients can be adopted in the quasi-steady theory proposed by Den Hartog ([2]) to estimate indirectly the critical velocity. This approach is the most popular due to its simplicity, but is based upon some fundamental hypotheses that are not always rigorously fulfilled. Moreover, the evaluation of static aerodynamic coefficients is affect by large uncertainties, and this is testified by the great variability in the results proposed by different experimental campaigns in different wind tunnels, even if carried out in the same flow conditions (Reynolds number, turbulence, blockage) ([5]).

Another practicable way is testing rigid bodies oscillating according to an imposed motion with pressure measurements. The motion-excited forces can be determined directly from the measurements, and an estimation of the critical flow velocity can be carried out through an unsteady formulation of the motion-induced forces. The difficulty in controlling all the experimental conditions, the necessarily finite length of the measurements and the inadequacy of the models used to fit the data in reproducing perfectly the physics of the problem are all sources of uncertainties, which obviously reflect into a correct estimation of the critical velocity.

The main purpose of this work is to investigate the uncertainty in the assessment of galloping instability by comparing the two described approaches. The uncertainty related to the quasi steady theory has been studied collecting different documented experimental results obtained in different wind tunnel tests. On the other hand, an experimental campaign involving pressure measurements on a rigid square prism in controlled motion has been carried out in the wind tunnel at the University of Genova. The uncertainties in the identification of aeroelastic forces are related to a single experimentation developed in only one facility and have been characterized by a statistical analysis. Therefore, the uncertainties in the assessment of galloping instability have a different nature. Nevertheless, focusing on a simple case study reproducing a slender structure with aerodynamic properties estimated by experimental tests, a qualitative and comparative analysis can be carried out. The results have been compared and critically discussed in term of reliability of the mechanical system in respect to galloping instability.

2 GALLOPING LINEAR INSTABILITY ANALYSIS

The present section provides some theoretical background to analyze the linear stability of a generic 2-dimensional bluff body with respect to plunge galloping. This aeroelastic phenomenon, referred to as classical galloping, is maybe the simplest one since involves only the displacement in the transverse direction with respect to the incoming flow velocity. Nevertheless, the problem can be formulated in different ways and in all cases substantial uncertainties may undermine a correct characterization of the phenomenon as well as the estimation of the instability conditions.

2.1 Quasi-Steady Linear Formulation

Let us consider a prismatic bluff body exposed to a uniform and constant cross-flow with velocity U. The prism is elastically constrained and can move only along the cross-flow direction. Let assume that only transverse motion $y(t)$ is possible and that the oscillation is about the static equilibrium position (i.e. $y(t)$ is zero mean).

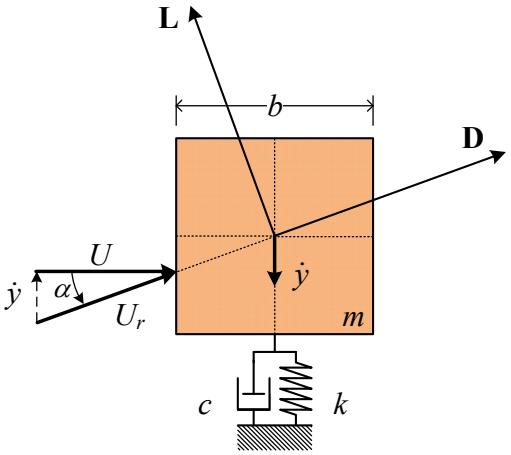

Figure 1: Mechanical system subjected to cross-flow velocity U.

The equation of motion of the prism can be written as:

$$m\ddot{y}(t) + c\dot{y}(t) + ky(t) = f_y(t) \tag{1}$$

where $y(t)$ is body displacement about the static equilibrium position, m is the mass, c is a damping factor, k is the stiffness and $f_y(t)$ is the projection of the aerodynamic forces (lift and drag) on the transverse direction.

The quasi-steady formulation is based upon the hypothesis that the characteristic time scale of the oscillating body is much slower than the characteristic fluid-dynamic time scale of the velocity fluctuation around the body. An explicit expression of this physical condition may be stated by comparing the frequency of oscillation n_s of the prism with the Vortex-Shedding (VS) frequency n_w, assuming that the following condition is fulfilled:

$$n_s \ll n_w = \frac{StU}{b} \tag{2}$$

being St the Strohual number and b a characteristic dimension of the prism. As a consequence of the time-scale separation, the aerodynamic forces acting on the prism oscillating with

the instantaneous velocity $\dot{y}(t)$ are equated to the forces acting on a fictitious fixed prism exposed to the flow-structure relative velocity U_r obtained by the composition of U and $\dot{y}(t)$ (Figure 1).

Operating in this way, the aerodynamic force remain expressed as a memory-less transformation of the effective angle of incidence α, or of the response velocity $\dot{y}(t)$. The linearization of this transformation about α=0 leads to the equation of motion [e.g. 7]:

$$m\ddot{y} + \left[c + \frac{1}{2}\rho U b \left(C_L' + C_D \right) \right] \dot{y} + ky = 0 \tag{3}$$

where ρ is the air density, C_D the drag coefficient for α=0 and C_L' the prime derivative with respect to α of the lift coefficient, estimated for α=0. The term $0.5\rho U b(C_L' + C_D)$ assumes the mechanical meaning of an aerodynamic damping factor. Galloping instability appears when the total damping goes to zero and an exponentially growing motion arises. This threshold is usually characterized by defining a critical velocity U_{cr} for which the aerodynamic damping term is equal to the structural damping term c, with opposite sign.

Following the quasi-steady formulation, the occurrence of a dynamic instability is estimated on the bases of experimental parameters assessed through static tests, namely drag and lift coefficients. For the square cross section at zero angle of incidence, C_L' is the most important term in the aerodynamic damping and can be estimated by fitting $C_L(\alpha)$ in the neighborhood of α=0 by a polynomial function ([1]).

Reference	a_g	Reference	a_g
[9]	3.11	[18]	2.70
	3.00		
[10]	2.69	[19]	3.50
	2.50		3.86
	2.72		4.10
	2.60		3.70
	2.40		
	2.30		
[11][12]	3.80	[20]	4.00
[13]	1.50	[21]	3.73
			3.60
[14]	4.00	[22]	2.05
	4.00		
	4.30		
[15]	3.85	[23]	2.69
	3.70		
	2.88		
[16]	2.20	[24]	1.2
	1.97		
[17]	5.40	[25]	1.13
	4.30		
[6]	3.42	[26]	1.78
$E\left[a_g\right]$	3.16	σ_{a_g}	1.02

Table 1: Aerodynamic parameters and relative test conditions for the square cylinder (after [5]).

In spite of the apparent simplicity of the experiment employed to estimate the parameter $a_g = C_D + C_L'$, a wide dispersion of this parameter is documented ([4], [5]). Table 1 summarizes some of the values of a_g presented in the literature for the case of square prisms with sharp corners in smooth flow.

Even if the experimental results reported in Table 1 have been filtered by considering only low-turbulence flow cases, the dispersion of the values appears very big (the coefficient of variation is about 0.3). This uncertainty reflects differences in the experimental setup used in different wind tunnels, blockage rate, Reynolds number, as well as the flow quality (intensity and scale of turbulence). On the other hand, the uncertainty is emphasized by the extremely high variations of the aerodynamic behavior that can be observed by applying even small variations of the angle of incidence. For this reason, an important role can be attributed to the positioning of the prism within the wind tunnel, the correct alignment and uniformity of the incoming flow, the correct geometric shape, surface finishing and corner shaping of the model.

2.2 Unsteady Linear Formulation

In the previous section, the aerodynamic forces have been modeled as a linear memory-less transformation of the body velocity. This assumption has two implications. First, the flow field around the body is modified instantaneously (without delay) by the body motion. Second, the instantaneous flow configuration appearing around the moving body can be reproduced in a static test by choosing an appropriate angle of incidence. While the first condition may be effectively reached when the body motion is slow enough, the fulfillment of the second condition depends on a large number of factors including the flow condition, the amplitude of the motion, the Reynolds number.

An unsteady linear model for the system described in the previous section can be formulated as:

$$m\ddot{y}(t) + c\dot{y}(t) + ky(t) = f_y(t) = \mathcal{H}\left[y(t)\right] \tag{4}$$

where $\mathcal{H}\left[\bullet\right]$ represents a linear operator (in general with memory) providing the aerodynamic forces, given the prism motion (this choice is purely conventional, since also a linear operator involving body velocity or acceleration could have been adopted). Equation (4) can be translated into the Laplace domain (assuming homogeneous initial conditions) as:

$$s^2 mY(s) + scY(s) + kY(s) = \frac{1}{2}\rho U^2 H(s) Y(s) \tag{5}$$

where $Y(s)$ is the Laplace transform of $y(t)$ and:

$$H(s) = \frac{F_y(s)}{\frac{1}{2}\rho U^2 Y(s)} \tag{6}$$

where $F_y(s)$ is the Laplace transform of $f_y(t)$. $H(s)$ can be interpreted as the transfer function of the linear system mapping the non-dimensional aerodynamic force $f_y(t)/(0.5\rho U^2 b)$ into the non-dimensional response $y(t)/b$.

If the motion of the prism is harmonic, with circular frequency ω, Eq.(5) can be rewritten in the time domain as:

$$m\ddot{y}(t) + \left[c - \frac{1}{2\omega}\rho U^2 I(\omega)\right]\dot{y}(t) + \left[k - \frac{1}{2}\rho U^2 R(\omega)\right] y(t) = 0 \tag{7}$$

where $R(\omega) = real(H(i\omega))$ and $I(\omega) = imag(H(i\omega))$. The functions $R(\omega)$ and $I(\omega)$ can be estimated through a controlled-motion test in which the prism is moved according to a sinusoidal motion with prescribed frequency.

In analogy with the quasi-steady formulation, the term $-0.5\rho U^2 I(\omega)/\omega$ can be interpreted as an aerodynamic damping. Analogously, the term $-0.5\rho U^2 R(\omega)$ can be interpreted as an aerodynamic stiffness.

It is well-known that for pitch-plunge aeroelastic systems, the aerodynamic stiffness has an important role. On the contrary, for the case of plunge single-dof system it is usually disregarded. This choice can be motivated through a simple dimensional analysis.

To this purpose, it is useful to introduce a scaled version of Eq.(7):

$$\ddot{y}(t) + 2\xi_s\omega_s\left[1 - \frac{1}{4\xi_s}\mu\widetilde{U}_s\widetilde{U}I(\omega)\right]\dot{y}(t) + \omega_s^2\left[1 - \frac{1}{2}\mu\widetilde{U}_s^2 R(\omega)\right]y(t) = 0 \tag{8}$$

in which the following non-dimensional quantities are introduced:

$$\xi_s = \frac{c}{2m\omega_s} \quad \omega_s = \sqrt{\frac{k}{m}} \quad \mu = \frac{\rho b^2}{m} \quad \widetilde{U} = \frac{U}{b\omega} \quad \widetilde{U}_s = \frac{U}{b\omega_s} \tag{9}$$

where ξ_s is the structural damping and ω_s is the natural frequency of the mechanical system; μ is a mass ratio, $\widetilde{U}$ is the reduced velocity and $\widetilde{U}_s$ is the reduced velocity corresponding to the resonance frequency.

From inspection of Eq.(8), it can be observed that the presence of the motion-excited forces reflects into corrective terms for the damping ratio and the natural frequency. A dimensional analysis suggests that, if $R(\omega)$ and $I(\omega)$ have the same order of magnitude, the corrective term of the natural frequency is at least two orders of magnitude smaller than the corrective term of damping, indeed:

$$O\left(\frac{\frac{1}{4\xi_s}\mu\widetilde{U}_s\widetilde{U}I(\omega)}{\frac{1}{2}\mu\widetilde{U}_s^2 R(\omega)}\right) = O\left(\frac{\widetilde{U}I(\omega)}{2\xi_s\widetilde{U}_s R(\omega)}\right) \tag{10}$$

in which ξ_s is typically of order 10^{-2} or 10^{-3}. This means that if the instability condition is reached, i.e. $0.25\mu\widetilde{U}_s\widetilde{U}I(\omega)/\xi_s = 1$, the corrective term of the stiffness is a small number.

Under the assumption of negligible aerodynamic stiffness and comparing Eq.(3) with Eq.(7) it is easy to demonstrate that the quasi-steady model corresponds to Eq.(8) with $R(\omega) = 0$ and

$$I(\omega) = -i\widetilde{\omega}a_g \tag{11}$$

$\widetilde{\omega}$ being the reduced circular frequency defined as $\widetilde{\omega} = \omega b/U$.

3 EXPERIMENTAL ESTIMATION OF MOTION-EXCITED FORCES

As explained in the previous sections, the galloping coefficient a_g adopted in quasi-steady theory can be estimated by wind tunnel tests on static models. On the other hand, the characterization of a linear relationship between the body motion and the aeroelastic forces is more complicated. One of the practicable way is to impose a controlled motion to the prism and measure the forces induced by the fluid.

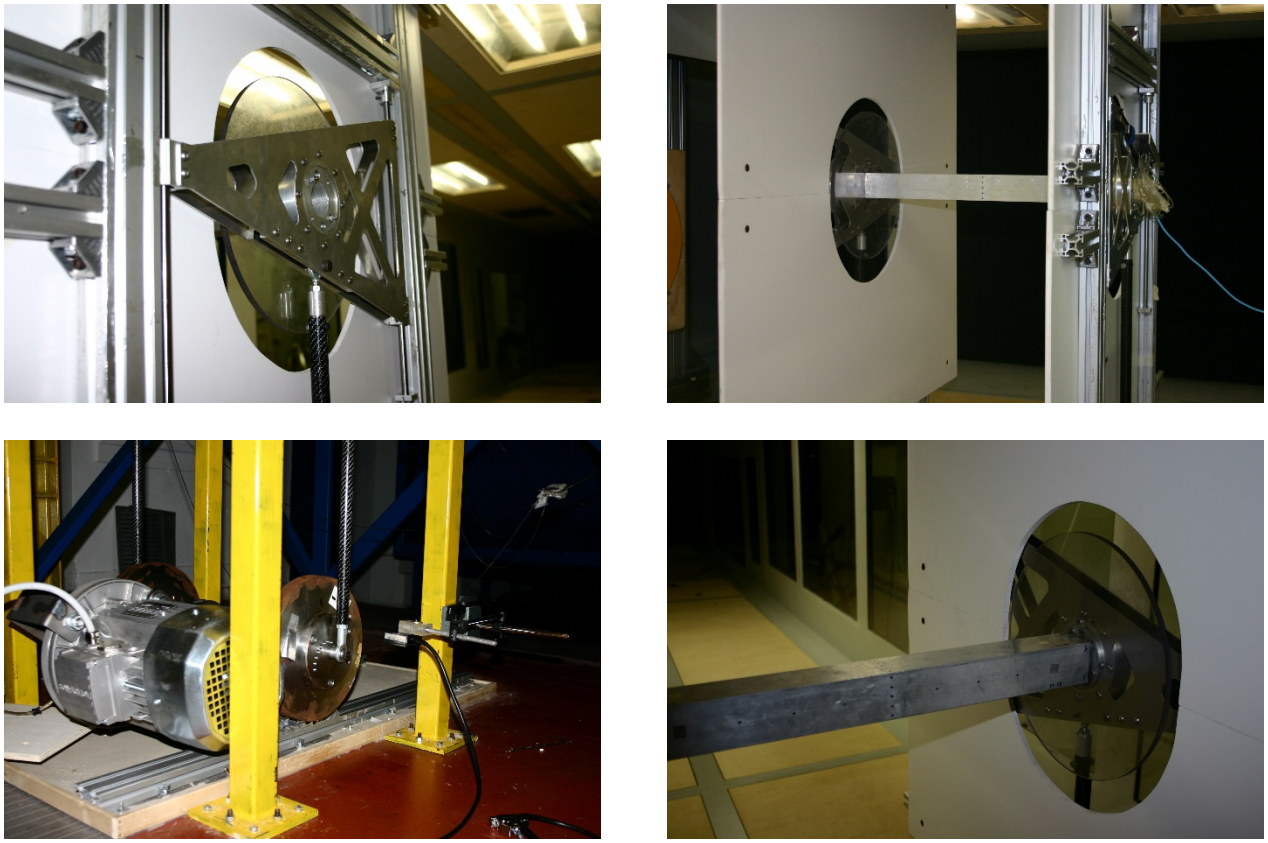

Figure 2: Experimental Setup

The experimental setup is constituted by a square prism moving in cross-flow direction according to a controlled harmonic motion. The size of the prism cross-section is $b = 50mm$ and its length is $L = 500mm$. The angle of incidence investigated is $\alpha = 0°$. The aerodynamic forces are estimated from the measurement of the pressure along an instrumented ring with 20 pressure taps located at the mid span of the model and connected to a pressure scanner mounted on-board. The harmonic motion is generated by a crankshaft driven by an electric motor regulated in velocity by a closed-loop controller. The model is connected to the shaft by a long rod pinned on a flywheel. The investigated motion frequency is in the interval of $n_m = 1 - 17.5Hz$. Three motion amplitudes are considered, namely Y = 5, 10, 15 *mm*, corresponding to the ratio b/Y = 10%, 20% and 30%. The mean wind velocity is U = 5m/s, corresponding to a Reynolds number $Re = 1.6 \cdot 10^4$ and Reduced Frequency (RF) $n_m b / U = 0.01 - 0.16$ or, equivalently, Reduced Velocity (RV) $U / n_m b = 6.25 - 100$ .The linear filter between imposed motion and aeroelastic forces can be defined as:

$$H(i\omega_m) = \frac{1}{\frac{1}{2}\rho Y U^2 T} E\left[\int_0^T F_y(t) e^{i\omega_m t} dt\right] \tag{12}$$

where $E[\bullet]$ represents the statistic average of the quantities evaluated for all the time intervals of length T in which the motion frequency is equal to $n_m = \omega_m / 2\pi$. The integral in Eq.(12) is a measure of the time correlation between the measured forces and the harmonics of the prism motion. Figure 3 shows the function $H(i\omega_m)$ in terms of amplitude and phase. The prediction given by the quasi-steady formulation is represented through a gray dashed line.

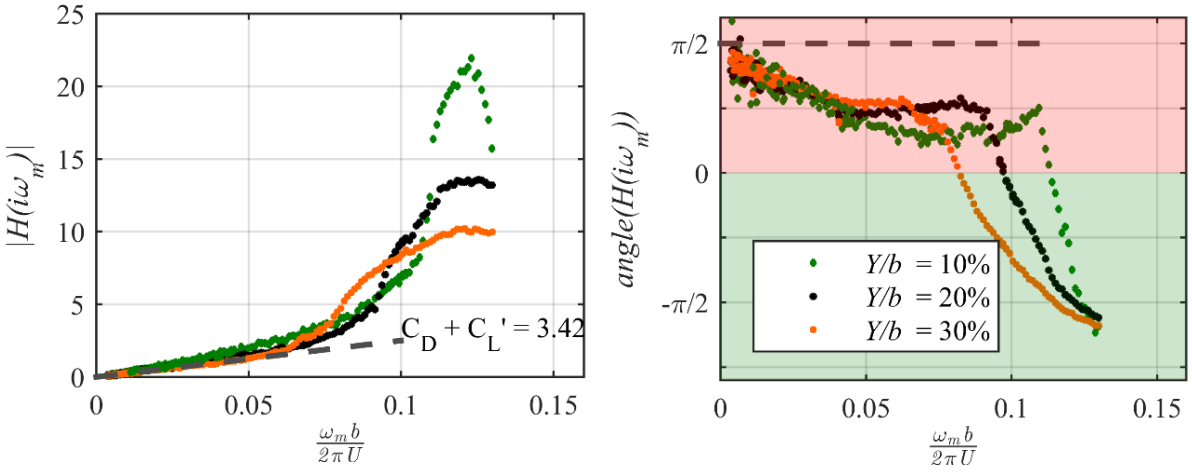

Figure 3: Amplitude and phase of the synchronous lift force for different motion amplitude. Stable region (green), unstable region (red). Quasi-steady prediction (black dashed line).

4 UNCERTAINTITES IN AEROELASTIC FORCES IDENTIFICATION

The imaginary and real parts of function $H(i\omega_m)$ are the cosine and sine transforms of the lift force respectively:

$$\hat{I}(\omega_m) = \frac{1}{\frac{1}{2}\rho Y U^2 T}\int_0^T F_y(t)\cos(\omega_m \mathrm{t})dt$$
$$\hat{R}(\omega_m) = \frac{1}{\frac{1}{2}\rho Y U^2 T}\int_0^T F_y(t)\sin(\omega_m \mathrm{t})dt \tag{13}$$

In practice, the measurement time T is finite due to experimental limitations, thus $\hat{I}(\omega_m)$ and $\hat{R}(\omega_m)$ can be computed relining only on a finite number of cycles $N = T\omega_m / 2\pi$; these estimations are denoted as $\hat{I}^{(N)}$ and $\hat{R}^{(N)}$.

For small RFs the lift force $F_y(\mathrm{t})$, measured for each different motion frequency, is an ergodic and stationary process, since the VS has a characteristic time scales much faster than the harmonic motion of the prism which is electronically controlled. Besides, for the same reason, the estimations of $\hat{I}^{(N)}$ and $\hat{R}^{(N)}$ calculated on non-overlapping time intervals are statistically independent. The consequence is that the statistic mean of $\hat{I}^{(N)}$ and $\hat{R}^{(N)}$ coincides with the exact values $I(\omega)$ and $R(\omega)$, while their standard deviations scale inversely with the square root of N, i.e.:

$$\sigma_{I^{(N)}} = \frac{1}{\sqrt{N}}\sigma_{I^{(1)}}; \qquad \sigma_{R^{(N)}} = \frac{1}{\sqrt{N}}\sigma_{R^{(1)}} \tag{14}$$

where $\hat{I}^{(1)}$ and $\hat{R}^{(1)}$ are the estimation of $I(\omega)$ and $R(\omega)$ obtained for $N = 1$.

Figure 4 shows the uncertainties in the estimation of $I(\omega_m)$ and $R(\omega_m)$ as a function of the RF and for different values of N. Black squares represents the sample averages of $\hat{I}^{(N)}$ and $\hat{R}^{(N)}$, while the errorbars represent their standard deviation as defined in Eq.(14).

Given mean and standard deviation, both the functions $\hat{I}^{(N)}$ and $\hat{R}^{(N)}$ can be modeled as random variables with Gaussian Probability Density Functions (PDF), accordingly with the Maximum Information Entropy principle [27].

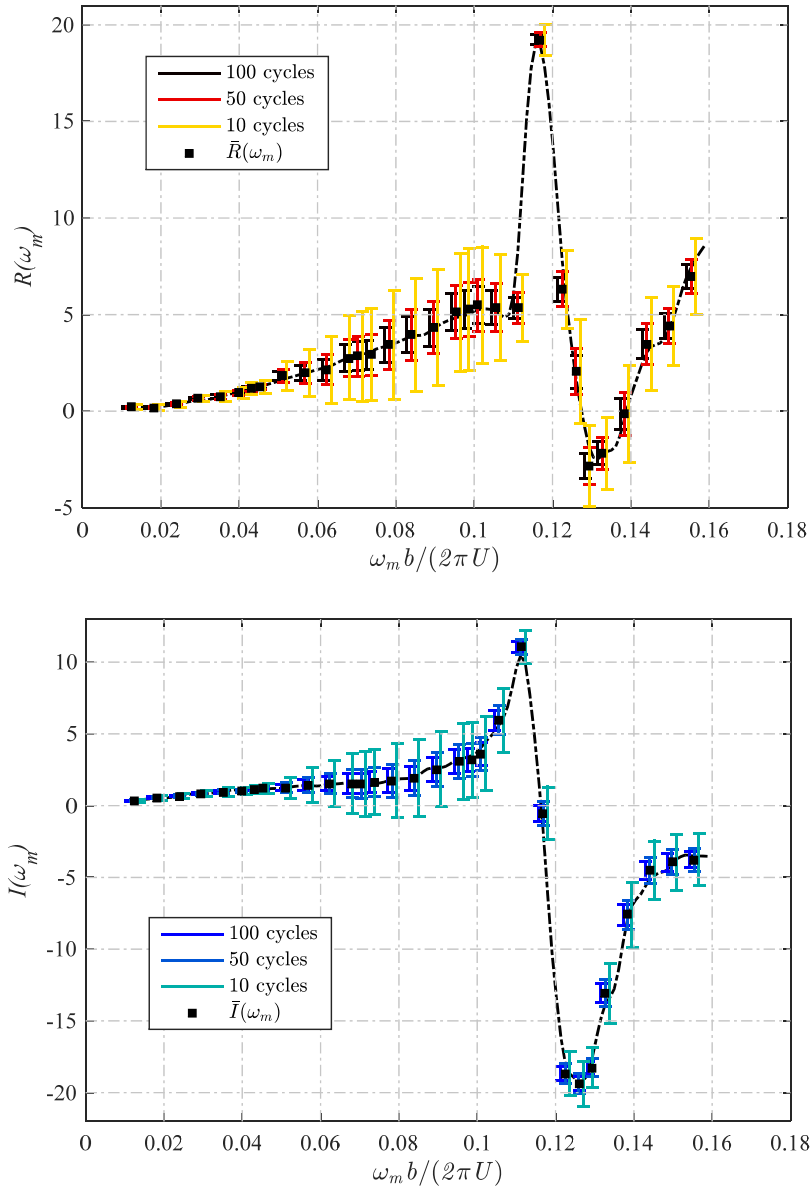

Figure 4: Errorbars of $I(\omega_m)$ and $R(\omega_m)$, for $Y/b = 10\%$ and for different values of N.

5 PROBABILISTIC MODELLING OF GALLOPING INSTABILITY: A SIMPLE CASE STUDY

The experimental results previously explained furnish a probabilistic model of the aeroelastic forces of a sharp edge square section in a smooth cross-flow. In order to investigate how these uncertainties, and the ones related to the evaluation of parameter a_g, reflect on the estimation of the galloping instability of a real structure a simple case study has been developed.

The structural system is a slender prismatic beam representative of a long bracing exposed to a steady flow with mechanical properties gathered in Table 2:

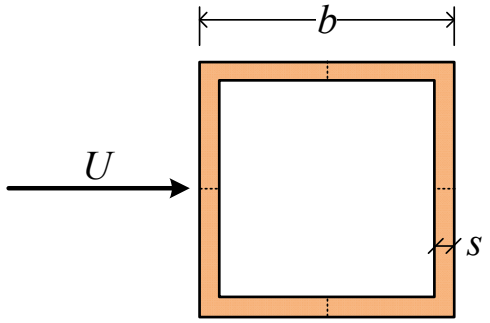

Parameter	Value
L	10m
b	0.2m
s	0.01m
m	60kg/m
n_s	6.31Hz
ξ_s	0.5%

Table 2: Case study.

5.1 Quasi-steady prediction

The critical velocity is defined by the quasi-steady theory as:

$$U_{QS} = \frac{8\pi\xi_s n_s m}{\rho b a_g} \tag{15}$$

Considering the aerodynamic parameter a_g as a random variable, the PDF of the critical velocity can be easily obtained as:

$$p(U_{QS}) = \left| -\frac{8\pi\xi_s n_s m}{\rho b u^2} \right| p_{a_g}\left(\frac{8\pi\xi_s n_s m}{\rho b u} \right) \tag{16}$$

where p_{a_g} is the PDF of a_g assumed according to the Gaussian model, with mean and standard deviation estimated from the data reported in Table 1. In this case the PDF of the critical velocity does not depend on the flow velocity, but only on the aerodynamic properties of the body, namely on a_g.

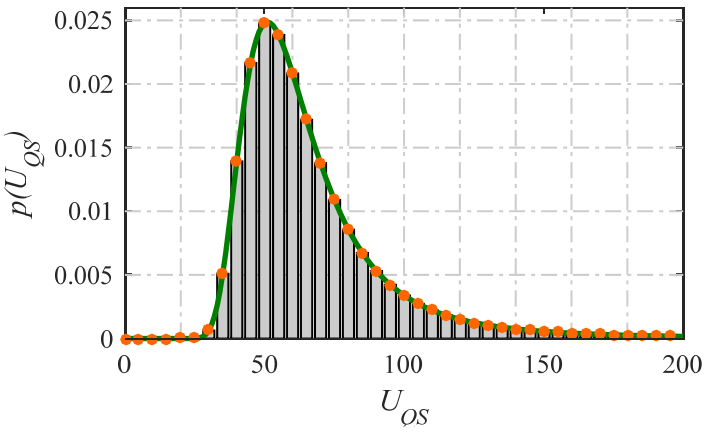

Figure 5: $p(U_{QS})$

5.2 Unsteady prediction

If the unsteady formulation is considered, the vertical oscillatory motion becomes unstable as soon as the total damping factor becomes negative, i.e. when the following identity holds:

$$C_a = \frac{1}{4\xi_s}\mu\widetilde{U}_s\widetilde{U}I(\omega_m) \simeq \frac{1}{4\xi_s}\mu\widetilde{U}_s^{\,2}I(\omega_m) = 1 \tag{17}$$

The oscillation frequency is equal to the natural frequency of the mechanical system since, as it has been discussed above, the modification of the stiffness due to the motion-induced forces is negligible. This implies that $\widetilde{U}_s \simeq \widetilde{U}$ and $\omega_s \simeq \omega_m$.

The critical velocity predicted by the unsteady formulation is given by:

$$U_{US} = \sqrt{\frac{4\xi_s b^2 \omega^2{}_s}{\mu I(\omega_s)}} = \sqrt{\frac{4\xi_s m \omega^2{}_s}{\rho I(\omega_s)}} \tag{18}$$

Considering all the variables as deterministic and assuming $I(\omega_s)$ as equal to the mean value of $\hat{I}^{(N)}$, (the black squares in Figure 4) the critical velocity $\bar{U}_{US}$ can be estimated directly from Eq.(18). On the other hand, if the uncertainty in the estimation of $\hat{I}^{(N)}$ is taken into account, the critical velocity U_{US} becomes a random variable whose PDF is expressed as:

$$p\left(U_{US} \mid \omega_s\right) = \left| -\frac{8\xi_s m \omega_s^2}{\rho u^3} \right| p_{\hat{I}^{(N)}(\omega_s)}\left(\frac{4\xi_s m \omega_s^2}{\rho u^2} \right) \tag{19}$$

The PDF of U_{US} is then a function of the motion frequency, assumed to be equal to the circular natural frequency of the mechanical system ω_s, and can be evaluated by fixing the reduced oscillation frequency $\widetilde{n}_s = \widetilde{\omega}_s / 2\pi = \omega_s b / 2\pi U$ or, equivalently, the reduced velocity $\widetilde{U} = 2\pi U / \omega_s b$. It is more convenient to rewrite the conditional probability function in (19) as:

$$p\left(U_{US} \mid U\right) = \left| -\frac{8\xi_s m \omega_s^2}{\rho u^3} \right| p_{\hat{I}^{(N)}(U)}\left(\frac{4\xi_s m \omega_s^2}{\rho u^2} \right) \tag{20}$$

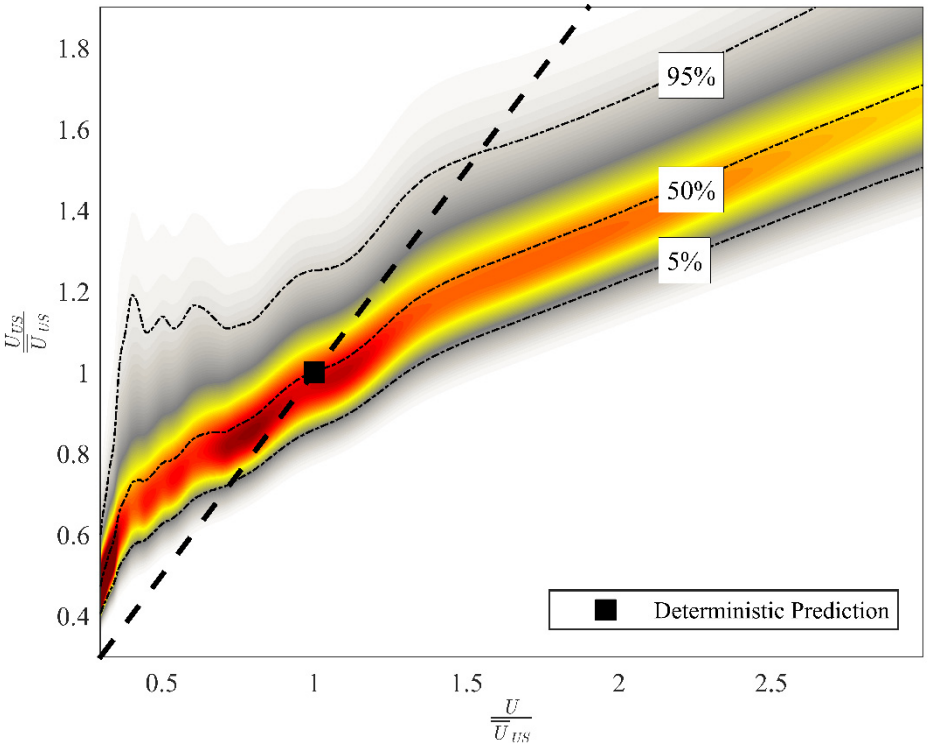

Figure 6: Map of $p(U_{US}, U)$ for N=50. Critical threshold (black dashed line).

in order to emphasize the conditioning on the flow velocity U. This conditional PDF furnishes the probability that, given a certain velocity of the flow, the system is stable or unstable, i.e. the probability that U is below or above the instability threshold defined by U_{US}. Observe that here, as first instance, the flow velocity U is assumed to be a deterministic quantity. Figure 6 shows a map of the conditional PDF $p\left(U_{US}\,|\,U\right)$. Both axes have been normalized with respect to the deterministic prediction $\bar{U}_{US}$. The black dashed line represents the stability threshold $U = U_{US}$, while the dash-dotted lines represent the 5%, 50% and 95% fractiles (conditioned on U), respectively. The intersection of the dashed line with the 50% fractile line coincides with the deterministic prediction. It should be noted that the mean value of U_{US} cannot be defined as it gets to infinity when no instability occurs.

When $U < \bar{U}_{US}$, the higher probability region is above the stability threshold while, on the contrary, when $U > \bar{U}_{US}$ the higher probability region is below the stability threshold.

Figure 7 shows the influence of N on the conditional PDF $p\left(U_{US}\,|\,U\right)$. For each value of N (1, 10, 50, 100, 10000) a confidence range of 80%, centered on the median, is displayed. As expected, the galloping velocity prediction tends to narrow around its median as the statistical information grows.

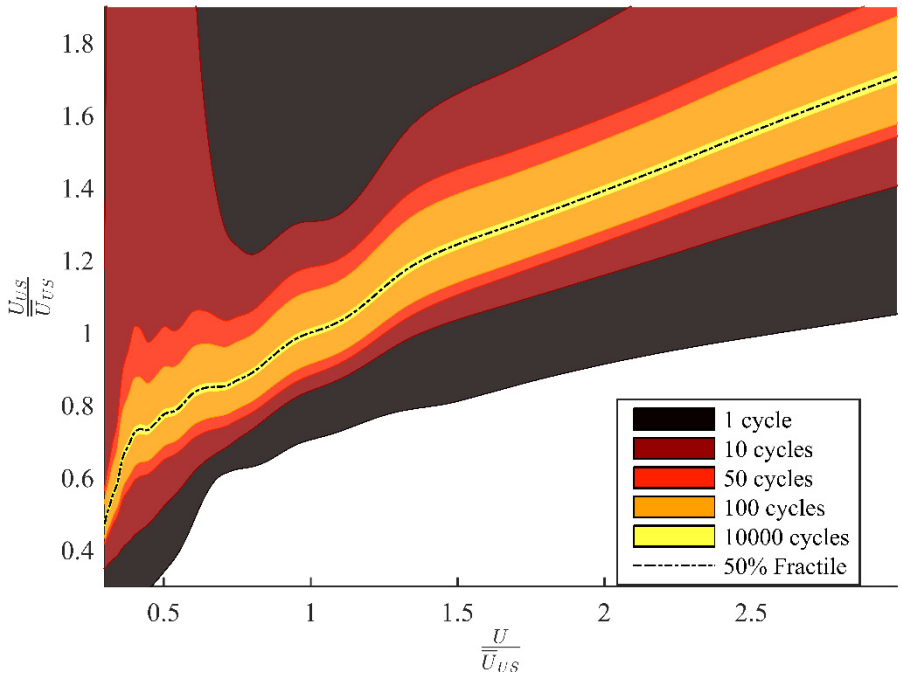

Figure 7: Influence of the number of cycles N on $p(U_{US}\,|\,U)$.

6 QUASI-STEADY VS. UNSTEADY PREDICTION

Using Bayes Theorem, the joint PDF of U_{US} and U is given by:

$$p(U_{US}, U) = p\left(U_{US}\,|\,U\right) p(U) \tag{21}$$

where $p(U)$ is the PDF of the wind velocity, where the corresponding cumulate density function (CDF) is assumed as [29]:

$$F_U(u) = \exp\left[-V_N \lambda A \frac{K}{C}\left(\frac{u}{C}\right)^{K-1} \exp\left(-\left(\frac{u}{c}\right)^{K}\right)\right] \tag{22}$$

where $A = 0.8428$, $K = 1.559$, $C = 5.258$ and $\lambda = 14959$ are numerical coefficients tuned with respect to the statistical analysis provided by [30] referring to Genova Expo area, V_N is the nominal life of the structure and is assumed equal to 100 years and $p(U) = \partial F_u(\mathrm{U}) / \partial u$. Figure 8 shows the joint PDFs of (U_{US}, U) for both unsteady (a) and quasi-steady (b) formulations. Both axes have been normalized with respect to $\bar{U}_{US}$. The dashed line represents the stability threshold. It appears that quasi-steady formulation tends to overestimate the critical velocity with respect to unsteady formulation. Moreover, the high-probability region is very wide, and consequently the prediction is more uncertain. This is not due to the modelling accuracy, but is a direct consequence of the great variability of the galloping parameter a_g. On the other hand, the smaller dispersion of the unsteady prediction is due to statistical uncertainties, due to the finite measurement length and to the experimental conditions.

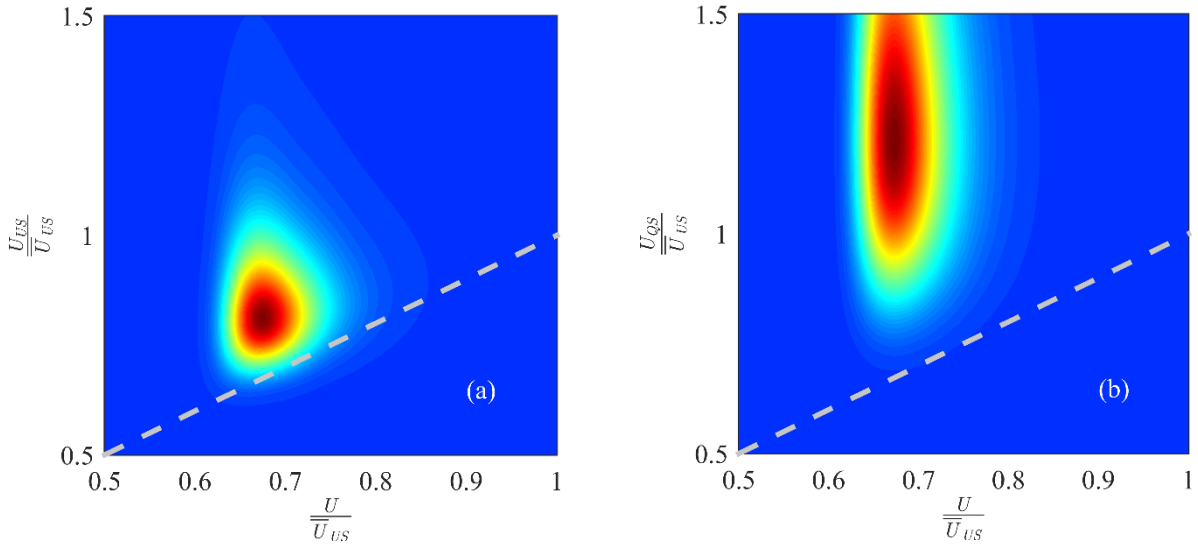

Figure 8: Map of $p(U_{US}, U)$ for N=50 (a) and $p(U_{QS}, U)$ (b). Critical threshold (gray dashed line).

Defining a failure margin M as:

$$M = \frac{U_{cr} - U}{U_{cr}} \qquad \left(U_{cr} = U_{US}, U_{QS}\right) \tag{23}$$

the same comparison can be made in terms of the failure PDF p_M defined as [28]:

$$p_M(m \mid V_N) = \frac{\partial}{\partial m} \iint_{\Delta D_M} p\left(U_{cr}, U\right) du_{cr} du \tag{24}$$

where ΔD_M is the region of the plane (U_{cr}, U) such that $m < M < m + dm$.

Figure 9 shows the p_M evaluated for both unsteady and quasi-steady predictions. It can be observed that the function M, as defined in (23), may assume values in the range $(-\infty; 1]$, where $M = 0$ corresponds to $U = U_{cr}$. It appears again clear that the quasi-steady formulation tends to overestimate the critical velocity and that this value is affected by large uncertainties.

The uncertainty of the prediction obtained using the unsteady formulation is relatively lower and obviously depends on the length of the measurements.

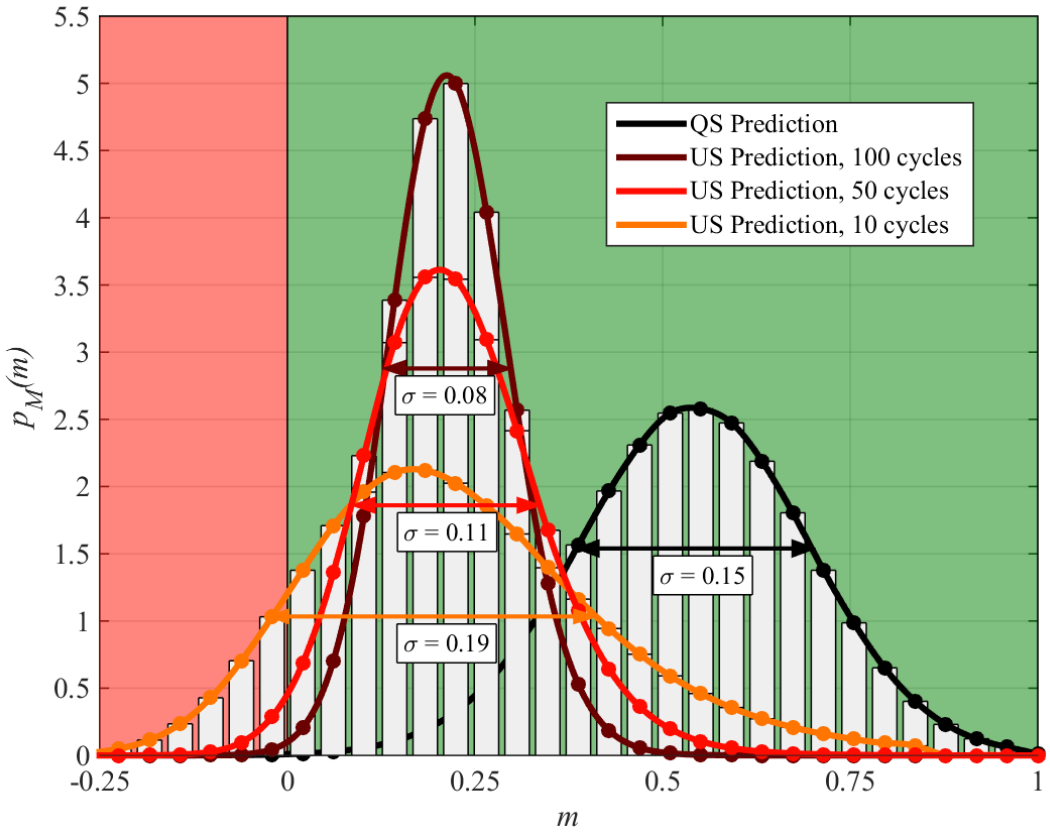

Figure 9: $P_M(m \mid V_N)$ for quasi-steady and unsteady predictions. Safety region (green) and failure region (red).

7 CONCLUSIONS

- The estimation of the galloping critical velocity is heavily uncertain due to errors related to several sources. Statistical errors depends on the finite sample available from experiments; modelling errors may derive from assumptions like in the quasi-steady formulation; other errors comes from experimental imperfections and reflect into a laboratory-to-laboratory variation of the measurements.
- If the quasi-steady formulation is applied, measurement uncertainties can be easily propagated to assess the uncertainty of the critical instability velocity. On the other hand, this operation is not trivial in case the unsteady formulation is adopted.
- The effect of the statistical error in the unsteady critical velocity can be estimated adopting some statistical assumptions that are reasonable in the low reduced-velocity range.
- The comparison between quasi-steady and unsteady prediction reveals systematic discrepancies, as well as a substantially different statistical variability. However, on the latter issue it must be observed that the data used in the present analysis include the laboratory-to-laboratory variation only for the quasi-steady formulation. This point may, at least partially, justify the larger dispersion of the results obtained by the quasi-steady formulation.

REFERENCES

[1] G.V. Parkinson, J.D. Smith, The square prism as aeroelastic non-linear oscillator, *The Quarterly Journal of Mechanics and Applied Mathematics,* **17** (2), 225-239.

[2] J.P.D.Hartog, *Transmission line vibration due to sleet*, Transactions of AIEE, 51, pp.1074-1076.

[3] L. Carassale, A. Freda and L. Banfi, Qualitative analysis of the motion-excited forces acting on a square prism, *XIII Conference of the Italian Association for Wind Engineering (IN-VENTO 2014)*, Genova, Italy, 22-25 June, 2014.

[4] L.C. Pagnini and G. Piccardo, Uncertainties in the evaluation of galloping oscillations, *14th International Conference on Wind Engineering (ICWE 14)*, Puerto Alegre (Brasil), June 12-26, 2015 (submitted).

[5] C. Mannini, A.M Marra and G.Bartoli, VIV-galloping instability of rectangular cylinders: Review and new experiments, *Journal of Wind Engineering and Industrial Aerodynamics*, **132**, pp. 109-124, 2014.

[6] A. Freda, L. Carassale, G. Piccardo, Aeroelastic crosswind response of sharp-edge square prisms: experiments versus theory, *14th International Conference on Wind Engineering (ICWE 14)*, Puerto Alegre (Brasil), June 12-26, 2015 (submitted).

[7] L. Carassale, A. Freda, and L. Banfi, Motion-excited forces acting on a square prism: a qualitative analysis, *14th International Conference on Wind Engineering (ICWE 14)*, Puerto Alegre (Brasil), June 12-26, 2015 (submitted).

[8] M. Païdoussis, S. Price and E. de Langre, *Fluid-Structure Interactions: Cross-Flow-Induced Instabilities,* Cambridge University Press, New York, USA, 2010.

[9] P.N.H. Brooks, *Experimental Investigation of the Aeroelastic Instability of Bluff Two-Dimensional Cylinders* (Master's thesis). University of British Columbia, Vancouver, Canada, 1960.

[10] J.D. Smith, *An Experimental Study of the Aeroelastic Instability of Rectangular Cylinders* (Master's thesis). University of British Columbia, Vancouver, Canada, 1962.

[11] Y. Nakamura, T. Mizota, Torsional flutter of rectangular prisms, *Journal of Engineering Mechanics,* **101(2)**, 125–142, 1975.

[12] Y. Nakamura, T. Mizota, Unsteady lifts and wakes of oscillating rectangular prisms. *Journal of Engineering Mechanics*, **101(6)**, 855–871, 1975.

[13] V. Mukhopadhyay, J. Dugundji, Wind excited vibration of a square section cantilever beam in smooth flow, *Journal of Sound and Vibration*, **45(3)**, 329–339, 1976.

[14] Y. Nakamura, Y. Tomonari, Galloping of rectangular prisms in a smooth and in a turbulent flow, *Journal of Sound and Vibration,* **52(2)**, 233–241, 1977.

[15] M.A. Wawzonek, *Aeroelastic Behavior of Square Section Prisms in Uniform Flow* (Master's thesis). University of British Columbia, Vancouver, Canada, 1979.

[16] G. Schewe, Untersuchung der aerodynamischen Kräfte,die auf stumpfe Profile bei großen Reynolds–Zahlen wirken, *Dfvlr-mitt*. 84-19, Deutsche Forschungs- und Versuchsangstalt für Luft- und Raumfahrt, 1984.

[17] P.W. Bearman, I.S. Gartshore, D.J. Maull, G.V. Parkinson, Experiments on fluid-induced vibration of a square-section cylinder, *Journal of Fluid and Structure,* **1(1)**, 19–34, 1987.

[18] ECCS, *Recommandations pour le Calcul des Effets du Vent sur les Constructions, deuxième edition*, European Convention for Constructional Steelwork (ECCS)—Comité Technique 12 'Vent', 1987.

[19] S.C. Luo, P.W. Bearman, Predictions of fluctuating lift on a transversely oscillating square-section cylinder, *Journal of Fluid and Structure,* **4(2)**, 219–228, 1990.

[20] C.W. Knisely, Strouhal numbers of rectangular cylinders at incidence: a review and new data, *Journal of Fluid and Structure,* **4(4)**, 371–393, 1990.

[21] C. Norberg, Flow around rectangular cylinders: pressure forces and wake frequencies, *Journal of Wind Engineering and Industrial Aerodynamics,* **49(1–3)**, 187–196, 1993.

[22] S.C. Luo, M.G. Yazdani, Y.T. Chew, T.S. Lee, Effects of incidence and afterbody shape on flow past bluff cylinders, *Journal of Wind Engineering and Industrial Aerodynamics ,* **53(3)**, 375–399, 1994.

[23] I. Robertson, L. Li, S.J. Sherwin, P.W. Bearman, A numerical study of rotational and transverse galloping rectangular bodies, *Journal of Fluid and Structures,* **17(5)**, 681–699, 2003.

[24] EN 1991-1-4, *Eurocode1 - Actions on Structures - Parts 1–4: General Actions - Wind Actions*, 2010.

[25] C. Borri, S. Zhou, Z. Chen, Coupling investigation on vortex-induced vibration and galloping of rectangular cylinders, *In: Proceedings of the Seventh International Colloquium on Bluff Body Aerodynamics and Applications*, Shanghai, China, September 2–6, 2012

[26] A. Joly, S. Etienne, D. Pelletier, Galloping of square cylinders in cross-flow at low Reynolds numbers. *Journal of Fluid and Structures,* **28**, 232–243, 2012.

[27] SF. Gull , Bayesian inductive inference and maximum entropy, *In Maximum Entropy and Bayesian Methods*, Skilling J (ed.), Kluwer Academic Publishers, Dordrecht, Holland, 53–74, 1989.

[28] A. Papoulis, *Probability, Random Variables and Stochastic Processes, 3rd Edition,* McGraw Hill, 1991.

[29] G. Solari, Wind speed statistics, in *Modelling of atmospheric flow fields*, Lalas, D.P., Ratto, C.F. (Edd.), World Scientific, Singapore, 1996.

[30] AA.VV., *Analisi del vento di progetto presso il Padiglione B della Fiera di Genova*, Dipartimento di Ingegneria delle Costruzioni, dell'Ambiente e del Territorio, Università degli Studi di Genova, 12 giugno 2007